Effect of cavity flow control on high-speed train pantograph and roof aerodynamic noise

Article *in* Railway Engineering Science · March 2020

DOI: 10.1007/s40534-020-00205-y

CITATIONS
37

READS
1,727

3 authors:

Hogun Kim
University of Southampton
6 PUBLICATIONS **93** CITATIONS
SEE PROFILE

Zhiwei Hu
University of Southampton
101 PUBLICATIONS **1,897** CITATIONS
SEE PROFILE

David Thompson
University of Southampton
541 PUBLICATIONS **14,163** CITATIONS
SEE PROFILE

PROCEEDINGS OF THE ROYAL SOCIETY A

Proc. R. Soc. A (2011) **467**, 144–165
doi:10.1098/rspa.2010.0172
Published online 30 June 2010

An acoustic analogy formulation for moving sources in uniformly moving media

By Alireza Najafi-Yazdi[1,*], Guillaume A. Brès[2] and Luc Mongeau[1]

[1]*Mechanical Engineering Department, McGill University, Montreal, Quebéc, Canada H3A2K6*
[2]*Exa Corporation, Brisbane, CA 94005, USA*

Acoustic analogy methods are used as post-processing tools to predict aerodynamically generated sound from numerical solutions of unsteady flow. The Ffowcs Williams–Hawkings (FW–H) equation and related formulations, such as Farassat's Formulations 1 and 1A, are among the commonly used analogies because of their relative low computation cost and their robustness. These formulations assume the propagation of sound waves in a medium at rest. The present paper describes a surface integral formulation based on the convective wave equation, which takes into account the presence of a mean flow. The formulation was derived to be easy to implement as a numerical post-processing tool for computational fluid dynamics codes. The new formulation constitutes one possible extension of Farassat's Formulation 1 and 1A based on the convective form of the FW–H equation.

Keywords: acoustic analogy; aeroacoustics; Ffowcs Williams–Hawkings equation

1. Introduction

As a branch of computational fluid dynamics (CFD), computational aeroacoustics (CAA) is dedicated to the study of aerodynamically generated sound. One common approach in CAA is to perform numerical simulations of the flow within a limited region of interest where sources are located, i.e. the nearfield. The sound radiated to the farfield is then calculated by solving a wave equation. This indirect approach, which is referred to as the acoustic analogy method in the literature, is often based on the assumption of linear propagation of waves from the nearfield to the farfield.

Depending on the motion of the observer and the ambient fluid speed, three possible problem types may be encountered, as summarized in table 1. The first type, referred to as *fly-over*, involves sound perceived by a stationary observer in a stationary ambient medium. The source may be either stationary or moving (e.g. the flight of an aircraft over a microphone array). The second type, referred to as *moving-observer*, deals with problems in which the observer is moving (e.g. microphone mounted on the fuselage of a helicopter or an aircraft). In the third type, referred to as *wind tunnel*, sound is received by a stationary observer in a moving medium such as sound measurements in wind tunnels.

*Author for correspondence (alireza.najafiyazdi@mail.mcgill.ca).

Received 30 March 2010
Accepted 26 May 2010

Table 1. Categories of problems usually encountered in design procedure. Sources can be either stationary or moving.

problem type	observer	ambient fluid	problem
1	stationary	stationary	fly-over
2	moving	stationary	moving-observer
3	stationary	moving	wind tunnel

A Galilean transformation may allow a problem of one type to be transformed into an equivalent problem of a different type. For example, a wind-tunnel problem in which the medium is moving at velocity $\mathbf{U}_0$ may be transformed into a moving-observer problem, where the observer and the source are translating at velocity $-\mathbf{U}_0$ with the medium being stationary. Such transformations are aimed at simplifying the problem and reducing the computation cost.

The Ffowcs Williams–Hawkings (FW–H) equation and related formulations, such as Farassat's Formulation 1 and 1A (Farassat 1975; Farassat & Succi 1980; Brentner 1997*a*), feature a relatively low computation cost, and they are fairly robust. These formulations have been successfully used for a wide range of fly-over and moving-observer problems (cf. Brentner & Farassat 2003; Lyrintzis 2003).

Formulations 1 and 1A do not explicitly take into account the presence of a mean flow for wind-tunnel problems. One common practice is to transform a given wind-tunnel problem into a moving-observer problem where the observer is assumed to be moving at a constant speed in a quiescent environment (Brentner & Farassat 2003). One alternative approach is to explicitly take the presence of a mean flow into account by solving a convective wave equation. Besides its mathematical elegance, such formulation helps in distinguishing mean flow effects on from sound generation phenomena.

The objective of the present paper is to present an extension of the classical FW–H equation and its subsequent formulations (Farassat's Formulation 1 and 1A) to wind-tunnel problems based on the solution of the convective wave equation. As such, it is referred to as Formulation 1C. The formulation is derived to be simple to implement and easy to parallelize. Formulation 1C is specifically designed to make efficient use of the nearfield data obtained from a CFD code.

The rest of the paper is organized as follows. The FW–H formulation for fly-over problems and the derivation of its convective form for wind-tunnel problems are reviewed in §2. The derivation of the new formulation is presented in §3. The numerical implementation and verification cases are discussed in §4.

2. Theoretical background

(*a*) *Acoustic analogy methods for fly-over problems*

The concept of the acoustic analogy was pioneered by Lighthill (1952) in his classical study of the sound generated by a turbulent jet (Lighthill 1954). Lighthill's idea was to recast the exact equations of motion, i.e. the conservation

Table 2. Nomenclature.

c_0	speed of sound in undisturbed medium
$f=0$	relation defining the position of the integral surface
g	retarded-time variable
H	heaviside function
$\mathbf{M}$	Mach number vector of the source
M_0	wind-tunnel Mach number
$\mathbf{n}$	unit vector normal to the surface
P_{ij}	stress tensor
p	pressure
R	Garrick triangle distance
$\mathbf{r}$	radiation vector, $\mathbf{r}=\mathbf{x}-\mathbf{y}$
r	distance between source and observer, $r=\|\mathbf{r}\|$
$\hat{\mathbf{r}}$	unit vector in the radiation direction
T_{ij}	Lighthill stress tensor
t	observer (reception) time
$\mathbf{U}_0$	wind-tunnel velocity
$\mathbf{u}$	fluid velocity
$\mathbf{v}$	surface velocity
$\mathbf{x}$	observer position
$\mathbf{y}$	source position
β	$\sqrt{1-{M_0}^2}$
δ	Dirac delta function
ρ	density
τ	source (emission) time
$\Box$	wave operator
subscript	
0	ambient quantity
i,j	vector component in fixed reference frame
n	projection in the normal direction
r	projection in the radiation direction
ret	quantity evaluated at the retarded time
superscript	
$*$	wind-tunnel quantity
$'$	perturbation quantity (e.g. $\rho'=\rho-\rho_0$)
$\cdot$	source-temporal derivative

of mass and momentum, as an inhomogeneous wave equation. The problem of calculating the turbulence-generated sound is then equivalent to solving the radiation of a distribution of sources into an ideal fluid at rest.

Lighthill's equation does not take into account the presence of solid surfaces in the field. A more general formulation which is applicable to the cases where a stationary solid surface is present in the flow field was developed by Curle (1955), and later generalized by Ffowcs Williams & Hawkings (1969) for moving and permeable surfaces. Di Francescantonio (1997) and Brentner & Farassat (1998) demonstrated the advantages of the permeable FW-H surface in CAA. The relationship between the permeable FW–H equation and Kirchoff methods (Farassat & Myers 1988; Lyrintzis 1994) was highlighted in Brentner & Farassat (1998).

The FW–H acoustic analogy involves enclosing the sound sources with a control surface that is mathematically represented by a function, $f(\mathbf{x}, t) = 0$. The acoustic signature at any observer position can be obtained from the FW–H equation

$$p'(\mathbf{x}, t) = \frac{\partial}{\partial t}\int_{f=0}\left[\frac{Q_i n_i}{4\pi|\mathbf{x}-\mathbf{y}|}\right]_{\tau_e} \mathrm{d}S - \frac{\partial}{\partial x_i}\int_{f=0}\left[\frac{L_{ij} n_j}{4\pi|\mathbf{x}-\mathbf{y}|}\right]_{\tau_e} \mathrm{d}S + \frac{\partial^2}{\partial x_i \partial x_j}\int_{f>0}\left[\frac{T_{ij}}{4\pi|\mathbf{x}-\mathbf{y}|}\right]_{\tau_e} \mathrm{d}V, \tag{2.1}$$

where $[\quad]_{\tau_e}$ denotes evaluation at the emission time τ_e. The source terms under the integral sign are

$$Q_i = \rho(u_i - v_i) + \rho_0 v_i, \tag{2.2}$$

$$L_{ij} = \rho u_i(u_j - v_j) + P_{ij}, \tag{2.3}$$

and T_{ij} is referred to as Lighthill's stress tensor,

$$T_{ij} = \rho u_i u_j + [(p - p_0) - c_0^2(\rho - \rho_0)]\delta_{ij} - \sigma_{ij}. \tag{2.4}$$

The vectors $\boldsymbol{u}$ and $\boldsymbol{v}$ are the flow and the surface velocities, respectively. See table 2 for the definition of other quantities. The compression tensor P'_{ij} is defined as

$$P_{ij} = (p - p_0)\delta_{ij} - \sigma_{ij}. \tag{2.5}$$

The third term integral should be evaluated in the region outside of the surface, $f > 0$, to account for the contribution of sound sources outside the FW–H surface. If the FW–H surface coincides with stationary solid boundaries, the flow velocity, $\mathbf{u}$, is equal to the surface velocity $\mathbf{v}$, which reduces the FW–H equation to Curle's equation (cf. Howe 1998).

The presence of both temporal and spatial derivatives with respect to the observer frame of reference may raise some problems for the numerical implementation of the FW–H equation in the form of equation (2.1). The FW–H equation was later revisited by Farassat (1975), Farassat & Succi (1980) and Brentner (1986, 1997*b*) and new formulations that are better suited for numerical implementations were introduced. These formulations, known as Formulations 1 and 1A, are widely employed in rotor and propeller noise studies.

An important point to note in equation (2.1) is the distinction between the emission time and the observer time. The left-hand side (LHS) of equation (2.1) denotes the pressure fluctuation perceived by the observer, located at $\mathbf{x}$, at time t. Equation (2.1) implies that the observer pressure fluctuation is obtained through the superposition of contribution from spatially distributed sources denoted by right-hand side (RHS) terms. Elemental contributions from each source are obtained by evaluating the RHS at the emission time, τ_e, which is different from t. Different sources may also have different emission time values τ_e depending on their position relative to the observer.

(*b*) *Retarded time versus advanced time algorithms*

Two approaches may be followed for the numerical implementation of equation (2.1) based on the distinction between the emission and observer times. In the retarded time approach (Brentner 1986, 1997*b*; Brentner & Farassat 2003),

the solution is evolved in the observer time frame. In other words, the observer time t and location $\mathbf{x}$ are kept constant at each time step. The emission time is calculated for each source location, $\mathbf{y}$. The associated flow properties are obtained using a temporal interpolation to obtain the required information at the emission time τ_e. This approach requires uploading the flow-field variables of multiple simulation snapshots per each observer time step calculation. Thus, the retarded time approach involves a large memory usage and computational cost associated with the interpolations of the time-resolved CFD results.

In the advanced time approach (Leishman 1996; Lyrintzis & Xue 1997; Casalino 2003; Lyrintzis 2003), also known as the source time-dominant algorithm (Brentner & Farassat 2003), the source time is chosen as the primary variable to evolve the solution. At each flow-field time step, matrices of instantaneous flow properties from the CFD solution are loaded into memory. The RHS of equation (2.1) is then evaluated at each point in space along with the arrival time value (advanced time). The resulting contribution is then added to the time history of the pressure received by the observer at the proper advanced time. Once the contributions from all points in the flow field have been calculated, the flow properties at the next source time step are loaded. As the calculation is evolved along the source time axis, the observer's sound pressure history is constructed. The advanced time approach is better suited than the retarded time, when large datasets provided by CFD codes are used as input data. The source time algorithm results in significant reduction in memory requirement, and is intrinsically parallelizable (Brentner & Farassat 2003; Lyrintzis 2003). A comparison between the cost of the two approaches was reported by Brès *et al.* (2004).

(*c*) *Wind-tunnel problems*

The classical FW–H equation—equation (2.1)—and subsequent formulations 1 and 1A do not explicitly take into account the presence of a mean flow for wind-tunnel problems. One solution is to transform the given wind-tunnel problem into a moving-observer problem, where the observer is assumed to be moving at a constant speed in a quiescent environment. One alternative approach is to explicitly take the presence of a mean flow into account by solving a convective wave equation (cf. Morino 1974, 1985). The second approach explicitly takes the mean flow into account in a cohesive mathematical framework. The resulting formulation provides some physical insight on the mean flow effects on the propagation of acoustic waves, and the presumed sound generation mechanism. It may also help to relate the results from wind-tunnel measurements with those obtained from fly-over experiments. The formulation also allows the clarification of some derivation details. In particular, also working with the advanced time algorithm, Casalino (2003) suggested to change the temporal derivatives with respect to the observer time of the non-convective FW–H equation into a Lagrangian derivative:

$$\frac{\partial}{\partial t} \longrightarrow \frac{\partial}{\partial t} + \mathbf{U}_0 \frac{\partial}{\partial x_1}, \tag{2.6}$$

where x_1 is the direction of the mean flow. This seems to be in contradiction with Brentner & Farassat (2003) on using the Formulations 1 and 1A for the moving-observer problems. The formulation of the present paper circumvents this difficulty by directly taking into account the presence of a mean flow rather than solving a moving-observer problem.

(*d*) *The convective FW–H equation*

The derivation of the convective FW–H equation was first introduced by Wells & Han (1995). The original derivation of Wells & Han (1995) did not include the quadrupole noise term, and was for a moving-observer problem by considering a moving frame of reference. This situation is equivalent to a stationary observer in a moving medium, i.e. wind-tunnel problems. For the sake of completeness and to clarify the notation, the convective FW–H equation is directly derived for a wind-tunnel problem in this section. Moreover, the quadrupole noise term is retained.

Consider the motion of an acoustic perturbation in a medium moving at constant velocity $\mathbf{U}_0$. The flow velocity at each point is $\mathbf{U}_0 + \mathbf{u}$,[1] where $\mathbf{u}$ is the local perturbation velocity. The continuity equation,

$$\frac{\partial \rho}{\partial t} + \frac{\partial \rho(U_{0j} + \mathbf{u}_j)}{\partial x_j} = 0, \tag{2.7}$$

can be simplified to

$$\frac{\partial \rho'}{\partial t} + U_{0j}\frac{\partial \rho'}{\partial x_j} + \frac{\partial \rho u_j}{\partial x_j} = 0, \tag{2.8}$$

where the primed variables denote perturbed quantities. The conservation of momentum,

$$\frac{\partial}{\partial t}[\rho(U_{0i} + u_i)] + \frac{\partial}{\partial x_j}[\rho(U_{0i} + u_i)(U_{0j} + u_j)] = -\frac{\partial}{\partial x_j}[(p - p_0)\delta_{ij} - \sigma_{ij}], \tag{2.9}$$

is recast as

$$\frac{\partial}{\partial t}[\rho u_i] + U_{0j}\frac{\partial}{\partial x_j}[\rho u_i] + \frac{\partial}{\partial x_j}[(p - p_0)\delta_{ij} + \rho u_i u_j - \sigma_{ij}] = 0. \tag{2.10}$$

The closed surface is mathematically represented by $f(\mathbf{x}, t) = 0$ (cf. figure 1).[2] This surface may be stationary or moving.

Without loss of generality, f may always be defined such that $f(\mathbf{x}, t) > 0$ represents the region outside the surface, $f(\mathbf{x}, t) < 0$ represents the region enclosed by the surface and $|\nabla f| = 1$ on the surface. The latter assumption is not necessary, but makes the derivations easier (Farassat 1994; Brentner & Farassat 2003).

[1]The bold font is used to denote vector quantities. Such quantities are also denoted as tensors of rank one and follow Einstein's index notation.

[2]The surface $f(\mathbf{x}, t)$ does not need to coincide with the solid surface as shown in figure 1. Indeed, the surface can be considered permeable or solid depending on the problem at hand.

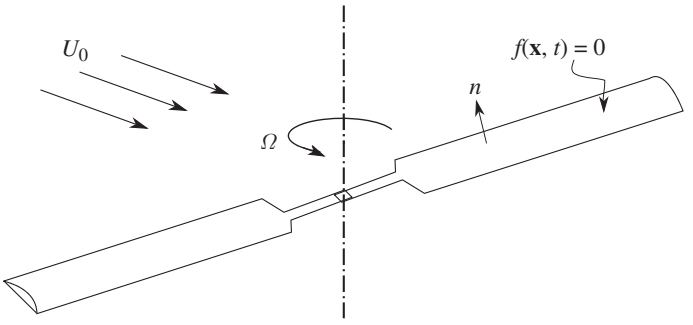

Figure 1. Flow over a rigid body whose motion is defined by $f(\mathbf{x}, t)$.

The continuity equation in the region outside the surface is then

$$H(f)\left[\frac{\partial \rho'}{\partial t} + U_{0j}\frac{\partial \rho'}{\partial x_j} + \frac{\partial \rho u_j}{\partial x_j}\right] = 0, \tag{2.11}$$

where H is the Heaviside function. Moving $H(f)$ inside the differential operators yields[3]

$$\frac{\partial H(f)\rho'}{\partial t} + U_{0j}\frac{\partial H(f)\rho'}{\partial x_j} + \frac{\partial H(f)\rho u_j}{\partial x_j} = \rho'\frac{\partial H(f)}{\partial t} + \rho' U_{0j}\frac{\partial H(f)}{\partial x_j} + \rho u_j\frac{\partial H(f)}{\partial x_j}. \tag{2.12}$$

Using

$$\frac{\partial H(f)}{\partial t} = \frac{\partial f}{\partial t}\delta(f) = -v_j n_j \delta(f) = -v_n \delta(f), \tag{2.13}$$

and

$$\frac{\partial H(f)}{\partial x_j} = \frac{\partial f}{\partial x_j}\delta(f) = n_j \delta(f), \tag{2.14}$$

equation (2.12) is recast as

$$\frac{\partial H(f)\rho'}{\partial t} + U_{0\,j}\frac{\partial H(f)\rho'}{\partial x_j} + \frac{\partial H(f)\rho u_j}{\partial x_j} = Q_j n_j \delta(f), \tag{2.15}$$

where

$$Q_j = [\rho(u_j + U_{0j} - v_j) + \rho_0(v_j - U_{0j})]. \tag{2.16}$$

Similarly, the conservation of momentum is written as

$$\frac{\partial}{\partial t}[H(f)\rho u_i] + c_0^2\frac{H(f)\partial \rho'}{\partial x_i} + U_{0j}\frac{\partial}{\partial x_j}[H(f)\rho u_i] = -\frac{\partial}{\partial x_j}\{H(f)\,T_{ij}\} + L_{ij}n_j\delta(f), \tag{2.17}$$

where

$$T_{ij} = \rho u_i u_j + [(p - p_0) - c_0^2(\rho - \rho_0)]\delta_{ij} - \sigma_{ij} \tag{2.18}$$

[3]Differentiation across a discontinuous function involves the use of generalized functions, also known as distributions in functional analysis and partial differential equations. See, for example, Renardy & Rogers (2004) or Farassat (1994, 2000) for an introduction to generalized functions.

is Lighthill's stress tensor and

$$L_{ij} = [\rho u_i(u_j + U_{0j} - v_j) + P_{ij})]. \tag{2.19}$$

In equation (2.18), the stress tensor P_{ij} is defined as

$$P_{ij} = (p - p_0)\delta_{ij} - \sigma_{ij}. \tag{2.20}$$

Differentiation of equation (2.15) with respect to time, calculation of the divergence of equation (2.17) and subtraction of the latter from the former yields

$$\left[\frac{\partial^2}{\partial t^2} - c_0^2\frac{\partial^2}{\partial x_j \partial x_j} + U_{0\,j}\frac{\partial^2}{\partial t \partial x_j}\right][H(f)\rho'] - U_{0\,j}\frac{\partial^2}{\partial x_i \partial x_j}[H(f)\rho u_i]$$
$$= \frac{\partial}{\partial t}[Q_j n_j \delta(f)] - \frac{\partial}{\partial x_i}[L_{ij} n_j \delta(f)] + \frac{\partial^2}{\partial x_i \partial x_j}[H(f)\, T_{ij}]. \tag{2.21}$$

Finally, equation (2.15) is used to replace the second term on the LHS of equation (2.21) and obtain the convective FW–H equation,

$$\left[\frac{\partial^2}{\partial t^2} - c_0^2\frac{\partial^2}{\partial x_j \partial x_j} + 2\,U_{0\,j}\frac{\partial^2}{\partial t \partial x_j} + U_{0i}\,U_{0j}\frac{\partial^2}{\partial x_i \partial x_j}\right][H(f)\rho']$$
$$= \left(\frac{\partial}{\partial t} + U_{0j}\frac{\partial}{\partial x_j}\right)[Q_k\ n_k\ \delta(f)] - \frac{\partial}{\partial x_i}\,[L_{ij} n_j \delta(f)] + \frac{\partial^2}{\partial x_i \partial x_j}[H(f)\, T_{ij}]. \tag{2.22}$$

The convective FW–H equation is an inhomogeneous convective wave equation similar to the well-known, classical, non-convective FW–H equation. The first two terms on the RHS of equation (2.22) are a (convective) monopole term, also known as thickness source, and a dipole term which is also called the loading source. The last term is a quadruple source term, which is typically small when compared with the other contributions. This term is also more challenging to compute and is often neglected. The specific form of the convective wave operator

$$\overline{\Box}^2 = \left[\frac{\partial^2}{\partial t^2} - c_0^2\frac{\partial^2}{\partial x_j \partial x_j} + 2\,U_{0j}\frac{\partial^2}{\partial t \partial x_j} + U_{0i}\,U_{0j}\frac{\partial^2}{\partial x_i \partial x_j}\right] \tag{2.23}$$

takes into account the presence of a mean flow and reduces to the simple wave operator when $\mathbf{U}_0 = 0$ as in the classical FW–H equation. The solution of equation (2.22) requires a Green's function that takes the presence of a mean flow into account, i.e. a convective Green's function. The thickness, Q_j, and loading, L_{ij} tensors include terms with the mean flow velocity and are slightly different from their counterparts in the non-convective FW–H equation. Lighthill's tensor definition retains the same as for the classical non-convective formulation.

Without loss of generality, it can be assumed that the mean flow velocity is along the positive x_1-direction.[4] Assuming a subsonic mean flow,

[4]If the mean flow is not along the x_1 direction, the reference frame can be rotated to satisfy this condition.

the three-dimensional free-space Green's function for the convective wave equation is (cf. eqns (1.91) and (1.92) of Blokhintsev 1956)

$$G(\mathbf{x}, t; \mathbf{y}, \tau) = \frac{\delta(\tau - t + R/c_0)}{4\pi R^*}, \tag{2.24}$$

where

$$R = \frac{-M_0(x_1 - y_1) + R^*}{\beta^2}, \tag{2.25}$$

$$R^* = \sqrt{(x_1 - y_1)^2 + \beta^2[(x_2 - y_2)^2 + (x_3 - y_3)^2]}, \tag{2.26}$$

and

$$\beta = \sqrt{1 - M_0^2}. \tag{2.27}$$

Using the above Green's function yields the solution to the convective FW–H differential equation,

$$\begin{aligned} c_0^2 \rho'(\boldsymbol{x}, t) = & \left[\frac{\partial}{\partial t} + U_0 \frac{\partial}{\partial x_1}\right] \int_{-\infty}^{t} \int_{\mathbb{R}^3} Q_j n_j \delta(f) \frac{\delta(g)}{4\pi R^*} \mathrm{d}^3 \boldsymbol{y}\, \mathrm{d}\tau \\ & - \frac{\partial}{\partial x_i} \int_{-\infty}^{t} \int_{\mathbb{R}^3} [L_{ij} n_j \delta(f)] \frac{\delta(g)}{4\pi R^*} \mathrm{d}^3 \boldsymbol{y}\, \mathrm{d}\tau \\ & + \frac{\partial^2}{\partial x_i \partial x_j} \int_{-\infty}^{t} \int_{\mathbb{R}^3} [H(f)\, T_{ij}] \frac{\delta(g)}{4\pi R^*} \mathrm{d}^3 \boldsymbol{y}\, \mathrm{d}\tau, \end{aligned} \tag{2.28}$$

where

$$g = \tau - t + \frac{R}{c_0}. \tag{2.29}$$

Equation (2.28) shows that the thickness of noise temporal derivative in the non-convective FW–H equation is indeed replaced by a Lagrangian derivative as suggested by Casalino (2003); however, this substitution is not sufficient to obtain correct results. In addition, Q_j and L_{ij} should be modified to include U_{0j} terms, as shown in equations (2.16) and (2.19). Moreover, the convective Green's function should be used, and not the free-space Green's function.

3. Formulation 1C

As for the classical non-convective FW–H equation, the numerical solution of the convective FW–H equation (2.28) is challenging because of the concurrence of spatial and temporal derivatives. This problem may be circumvented as presented next. The contribution of quadrupole noise terms is neglected in the following,[5] and the thickness and loading terms are treated separately.

[5]Di Francescantonio (1997) and Morgans *et al.* (2005) discuss in detail that the permeable control surface can be chosen, such that the important noise sources are enclosed without the need to calculate the quadrupole noise.

(*a*) *Thickness noise*

The thickness noise contribution, p'_T, is obtained from

$$4\pi p'_T = \left[\frac{\partial}{\partial t} + U_0\frac{\partial}{\partial x_1}\right]\int_{-\infty}^{t}\int_{\mathbb{R}^3} Q_j n_j \delta(f)\frac{\delta(g)}{R^*}\mathrm{d}^3\mathbf{y}\mathrm{d}\tau. \tag{3.1}$$

The surface $f=0$ may be defined in a frame of reference fixed to the surface, $\boldsymbol{\eta}$. Any point on the surface is defined by a fixed value of the variable, $\boldsymbol{\eta}$, irrespective of the motion of the surface. The motion of each point on the surface is then fully described in terms of the translation and the rotation of the $\boldsymbol{\eta}$ frame of reference. It is also assumed that the FW–H surface does not undergo deformation, expansion or contraction. Since the transformations

$$\mathbf{y} = \mathbf{y}(\boldsymbol{\eta}, \tau) \tag{3.2}$$

and

$$\boldsymbol{\eta} = \boldsymbol{\eta}(\mathbf{y}, \tau) \tag{3.3}$$

are isometric, the Jacobian of the transformation is unity. Hence, equation (3.1) may be written as:

$$4\pi p'_T = \left[\frac{\partial}{\partial t} + U_0\frac{\partial}{\partial x_1}\right]\int_{-\infty}^{t}\int_{\mathbb{R}^3} Q_j n_j \delta(f)\frac{\delta(g)}{R^*}\mathrm{d}^3\boldsymbol{\eta}\,\mathrm{d}\tau. \tag{3.4}$$

To obtain a formulation that is suitable for numerical implementation, the spatial derivative $\partial/\partial x_1$ must be converted into a temporal derivative. All terms in the integral are functions of $\boldsymbol{\eta}$ and τ only, with the exception of $\delta(g)/R^*$, which depends on $\boldsymbol{x}$ and t as well. The combination of

$$\frac{\partial}{\partial x_i}\left(\frac{\delta(g)}{R^*}\right) = \frac{1}{c_0}\frac{\partial R}{\partial x_i}\frac{\delta'(g)}{R^*} - \frac{\partial R^*}{\partial x_i}\frac{\delta(g)}{R^{*2}} = \frac{1}{c_0}\frac{\tilde{R}_i\delta'(g)}{R^*} - \frac{\tilde{R}^*_i\delta(g)}{R^{*2}} \tag{3.5}$$

and

$$\frac{1}{c_0}\frac{\partial}{\partial t}\left(\frac{\tilde{R}_i\delta(g)}{R^*}\right) = -\frac{1}{c_0}\left(\frac{\tilde{R}_i\delta'(g)}{R^*}\right) \tag{3.6}$$

yields

$$\frac{\partial}{\partial x_i}\left(\frac{\delta(g)}{R^*}\right) = -\frac{1}{c_0}\frac{\partial}{\partial t}\left(\frac{\tilde{R}_i\delta(g)}{R^*}\right) - \frac{\tilde{R}^*_i\delta(g)}{R^{*2}}, \tag{3.7}$$

where the radiation vector $\tilde{\mathbf{R}}$ is

$$\tilde{R}_1 = \frac{1}{\beta^2}(-M_0 + \tilde{R}^*_1), \quad \tilde{R}_2 = \frac{x_2 - y_2}{R^*}, \quad \tilde{R}_3 = \frac{x_3 - y_3}{R^*} \tag{3.8}$$

and

$$\tilde{R}^*_1 = \frac{x_1 - y_1}{R^*}, \quad \tilde{R}^*_2 = \beta^2\frac{x_2 - y_2}{R^*}, \quad \tilde{R}^*{}_3 = \beta^2\frac{x_3 - y_3}{R^*}. \tag{3.9}$$

These relations may be used to recast equation (3.1) as

$$4\pi p'_T = \frac{\partial}{\partial t}\int_{-\infty}^{t}\int_{\mathbb{R}^3} Q_j n_j \delta(f)\frac{\delta(g)}{R^*}\mathrm{d}^3\boldsymbol{\eta}\,\mathrm{d}\tau - M_0\frac{\partial}{\partial t}\int_{-\infty}^{t}\int_{\mathbb{R}^3} Q_j n_j \delta(f)\left(\frac{\tilde{R}_1\delta(g)}{R^*}\right)\mathrm{d}^3\boldsymbol{\eta}\,\mathrm{d}\tau - U_0\int_{-\infty}^{t}\int_{\mathbb{R}^3} Q_j n_j \delta(f)\frac{\tilde{R}_1^*\delta(g)}{R^{*2}}\mathrm{d}^3\boldsymbol{\eta}\,\mathrm{d}\tau. \tag{3.10}$$

The next step is to change the variable from τ to g. By definition, $\partial g/\partial\tau$ is obtained from

$$\frac{\partial g}{\partial \tau} = 1 + \frac{1}{c_0}\frac{\partial R}{\partial y_i}\frac{\partial y_i}{\partial \tau} = 1 - M_R, \tag{3.11}$$

where M_R is defined as

$$M_R = \frac{1}{c_0}\frac{\partial y_i}{\partial \tau}\tilde{R}_i = \frac{1}{c_0}v_i\tilde{R}_i. \tag{3.12}$$

Using equation (3.11), we have

$$\mathrm{d}\tau = \frac{1}{1-M_R}\mathrm{d}g. \tag{3.13}$$

Hence, equation (3.10) is simplified to

$$4\pi p'_T = \frac{\partial}{\partial t}\int_{f=0}\left[\frac{Q_j n_j}{R^*(1-M_R)}\right]_{\mathrm{ret}}\mathrm{d}\boldsymbol{\eta} - M_0\frac{\partial}{\partial t}\int_{f=0}\left[\frac{\tilde{R}_1 Q_j\, n_j}{R^*(1-M_R)}\right]_{\mathrm{ret}}\mathrm{d}\boldsymbol{\eta} - U_0\int_{f=0}\left[\frac{\tilde{R}_1^* Q_j n_j}{R^{*^2}(1-M_R)}\right]_{\mathrm{ret}}\mathrm{d}\boldsymbol{\eta}, \tag{3.14}$$

where $[\ldots]_{\mathrm{ret}}$ denotes the evaluation at the retarded (emission) time

$$\tau_{\mathrm{e}} = t - \left[\frac{R}{c_0}\right]_{\tau_{\mathrm{e}}}. \tag{3.15}$$

The quantity R is no longer the geometric distance between the observer and the source, but the *acoustic* distance between the two, as defined in equation (2.25) (Wells & Han 1995). In the limit of zero mean flow velocity, the acoustic distance and the geometric distance are equal. The observer temporal derivative, $\partial/\partial t$, may be evaluated numerically using a backward difference in time.

Some difficulties may arise in the reconstruction of the signal using the advanced time approach. The input flow properties are usually provided at equally spaced time steps in the source time domain; however, the uniform discretization of the source time domain does not necessarily yield a uniform discretization of the observer time domain because of the Doppler effect.

This inconvenience may be avoided by moving the observer temporal derivative inside the integral, and transforming it into a source temporal derivative (cf. appendix A for details of the derivation).

The thickness noise contribution to the farfield sound pressure is then equal to

$$\begin{aligned}4\pi p'_T = &\int_{f=0}\left[\frac{\dot{Q}_i n_i + Q_i \dot{n}_i}{R^*(1-M_R)^2}\right]_{\tau_e} \mathrm{d}\boldsymbol{\eta} + \int_{f=0}\left[\frac{-\partial R^*}{\partial\tau}\frac{Q_i\ n_i}{R^{*^2}(1-M_R)^2}\right]_{\tau_e}\mathrm{d}\boldsymbol{\eta}\\ &+\int_{f=0}\left[\frac{Q_i\ n_i}{R^*(1-M_R)^3}\frac{\partial M_R}{\partial\tau}\right]_{\tau_e}\mathrm{d}\boldsymbol{\eta}\\ &-M_0\int_{f=0}\left[\frac{\dot{\tilde{R}}_1 Q_i n_i + \tilde{R}_1\dot{Q}_i n_i + \tilde{R}_1 Q_i \dot{n}_i}{R^*(1-M_R)^2}\right]_{\mathrm{ret}}\mathrm{d}\boldsymbol{\eta}\\ &+M_0\int_{f=0}\left[\frac{\partial R^*}{\partial\tau}\frac{\tilde{R}_1 Q_i n_i}{R^{*^2}(1-M_R)^2}\right]_{\mathrm{ret}}\mathrm{d}\boldsymbol{\eta} - M_0\int_{f=0}\left[\frac{\partial M_R}{\partial\tau}\frac{\tilde{R}_1 Q_i n_i}{R^*(1-M_R)^3}\right]_{\mathrm{ret}}\mathrm{d}\boldsymbol{\eta}\\ &-U_0\int_{f=0}\left[\frac{\tilde{R}_1^* Q_i n_i}{R^{*^2}(1-M_R)}\right]_{\mathrm{ret}}\mathrm{d}\boldsymbol{\eta}. \end{aligned} \tag{3.16}$$

where dots over quantities denote temporal derivatives with respect to the source time. The term $\dot{Q}_i$ is obtained numerically, while other temporal derivatives are obtained either numerically or analytically.

(*b*) *Loading noise*

The loading noise is obtained from

$$4\pi p'_L = -\frac{\partial}{\partial x_i}\int_{-\infty}^{t}\int_{\mathbb{R}^3}[L_{ij}n_j\delta(f)]\frac{\delta(g)}{R^*}\mathrm{d}^3\mathbf{y}\,\mathrm{d}\tau. \tag{3.17}$$

As for the thickness noise, all terms under the integral are functions of $\boldsymbol{\eta}$ and τ only, with the exception of $\delta(g)/R^*$. Therefore, equation (3.7) is used to transform the spatial derivative, $\partial/\partial x_i$, into the observer temporal derivative, which yields

$$4\pi p'_L = \frac{\partial}{\partial t}\int_{-\infty}^{t}\int_{\mathbb{R}^3}\frac{1}{c_0}[L_{ij}n_j\delta(f)]\frac{\tilde{R}_i\delta(g)}{R^*}\mathrm{d}^3\mathbf{y}\,\mathrm{d}\tau + \int_{-\infty}^{t}\int_{\mathbb{R}^3}[L_{ij}n_j\delta(f)]\frac{\tilde{R}_i^*\delta(g)}{R^{*^2}}\mathrm{d}^3\mathbf{y}\,\mathrm{d}\tau. \tag{3.18}$$

Equation (3.13) is used to further simplify the above equation to

$$4\pi p'_L = \frac{1}{c_0}\frac{\partial}{\partial t}\int_{f=0}\left[\frac{L_{ij}n_j\tilde{R}_i}{R^*(1-M_R)}\right]_{\tau_e}\mathrm{d}\boldsymbol{\eta} + \int_{f=0}\left[\frac{L_{ij}n_j\tilde{R}_i^*}{R^{*^2}(1-M_R)}\right]_{\tau_e}\mathrm{d}\boldsymbol{\eta}. \tag{3.19}$$

It can be verified that letting $U_0 = 0$ recovers the loading noise term in Farassat's Formulation 1. The loading noise contribution may also be written in terms of source temporal derivatives as follows:

$$4\pi p'_L = \frac{1}{c_0}\int_{f=0}\left[\frac{\dot{L}_{ij}n_j\tilde{R}_i + L_{ij}\dot{n}_j\tilde{R}_i + L_{ij}n_j\dot{\tilde{R}}_i}{R^*(1-M_R)^2}\right]_{\tau_e} \mathrm{d}\boldsymbol{\eta} - \frac{1}{c_0}\int_{f=0}\left[\frac{\partial R^*}{\partial\tau}\frac{L_{ij}n_j\tilde{R}}{R^{*^2}(1-M_R)^2}\right]_{\tau_e} \mathrm{d}\boldsymbol{\eta} + \frac{1}{c_0}\int_{f=0}\left[\frac{\partial M_R}{\partial\tau}\frac{L_{ij}n_j\tilde{R}}{R^*(1-M_R)^3}\right]_{\tau_e} \mathrm{d}\boldsymbol{\eta} + \int_{f=0}\left[\frac{L_{ij}n_j\tilde{R}^*_i}{R^{*^2}(1-M_R)}\right]_{\tau_e} \mathrm{d}\boldsymbol{\eta}. \tag{3.20}$$

This equation is equivalent to the loading noise term of Farassat's formulation 1A, and is convenient for the implementation of the advance time algorithm.

(c) *The special case of 'wind tunnel'*

In the particular case where both the source and the observer are stationary in a wind tunnel, simplifications in Formulation 1C lead to increased computational efficiency.

In Formulation 1C, the distances R and R^*, defined by equations (2.25) and (2.26), are constant and do not vary with time. The same observation applies to the radiation vector components $\hat{R}_i$, the local normal vector components n_i, and $M_R = 0$. Therefore, these variables can be evaluated and stored at preprocessing, rather than being computed at every time step, and their source temporal derivative is zero. Likewise, the source Mach number $\mathbf{M}$ and the unit normals $\mathbf{n}$ are not functions of time, so $\dot{M}_r = 0$ and $\dot{n} = 0$. These simplifications lead to the following expressions for the thickness noise

$$4\pi p'_T = \int_{f=0}\left[(1-M_0)\frac{\dot{Q}_i n_i}{R^*} - U_0\frac{\tilde{R}^*_1 Q_i n_i}{R^{*^2}}\right]_{\tau_e} \mathrm{d}\boldsymbol{\eta}, \tag{3.21}$$

and the loading noise

$$4\pi p'_L = \int_{f=0}\left[\frac{1}{c_0}\frac{\dot{L}_{ij}n_j\tilde{R}_i}{R^*} + \frac{L_{ij}n_j\tilde{R}^*_i}{R^{*^2}}\right]_{\tau_e} \mathrm{d}\boldsymbol{\eta}. \tag{3.22}$$

The terms containing R^{*^2} vanish quickly in the farfield as $R^* \longrightarrow \infty$, and thus they are significant only in the nearfield. It is important to note that the amplitude of the thickness term contribution to the farfield noise decreases with increasing mean flow Mach number. Therefore, loading noise becomes the dominant source term for high Mach number flows.

4. Numerical implementation and verification

Formulation 1C was implemented in an object-oriented code written in C++. The input to the code is a surface mesh, which defines the FW–H surface, and the time-accurate flow solution obtained from a distinct CFD code. Surface elements (panels) may be triangular, quadrilateral or polygonal. The flow properties are specified at the centre of each panel (for first-order accuracy) or at the vertices of the panel (for higher order accuracy) at each time step of the solution. The temporal derivatives are obtained from a finite difference approximation. Finite-element type shape functions are used for the spatial interpolation. The integral terms are then obtained from a Gaussian quadrature with an appropriate number of points to obtain the desired order of accuracy. The FW–H code was written based on the advanced time algorithm. The canonical problems of sound radiation by a monopole and a dipole in a uniform mean flow were solved for the numerical verification of the formulation. Source terms were computed over a fictitious, closed surface surrounding the source.

In all test cases, the mesh resolution of the FW–H surface and the source and observer time steps are chosen such that the wavelength and period of the radiated waves are resolved with at least eight points.

(*a*) *Test case 1. Stationary monopole in a moving medium*

The monopole sound-field is characterized by a simple harmonic velocity potential function (Lockard 2002)

$$\phi(\mathbf{x}, t) = \frac{A}{4\pi R^*} \exp\left[\mathrm{i}\omega\left(t - \frac{R}{c_0}\right)\right]. \tag{4.1}$$

The induced particle velocity is obtained from

$$\mathbf{u}(\mathbf{x}, t) = \nabla\phi(\mathbf{x}, t). \tag{4.2}$$

The induced pressure and density, for the case with a mean flow U_0 along the x_1-direction, are related to the velocity potential through

$$p'(\mathbf{x}, t) = -\rho_0\left[\frac{\partial}{\partial t} + U_0\frac{\partial}{\partial x_1}\right]\phi \tag{4.3}$$

and

$$\rho'(\mathbf{x}, t) = \frac{p'}{c_0^2}, \tag{4.4}$$

respectively.

To keep a focus on the formulation and its implementation, and to avoid any bias related to the accuracy of the flow solver, the flow properties on the FW–H surface were obtained from the exact solution of the flow field generated by the monopole, i.e. equations (4.1)–(4.4). These properties were then used as the input to the code.

The monopole was located at the origin of the coordinate system. The velocity potential amplitude was $A = 1\,\mathrm{m}^2\,\mathrm{s}^{-1}$. The pulsation frequency was 5 Hz. The radiated sound pressure was calculated at a geometrical distance of $340l$ from the source, where the characteristic length of the FW–H surface, l, was set to

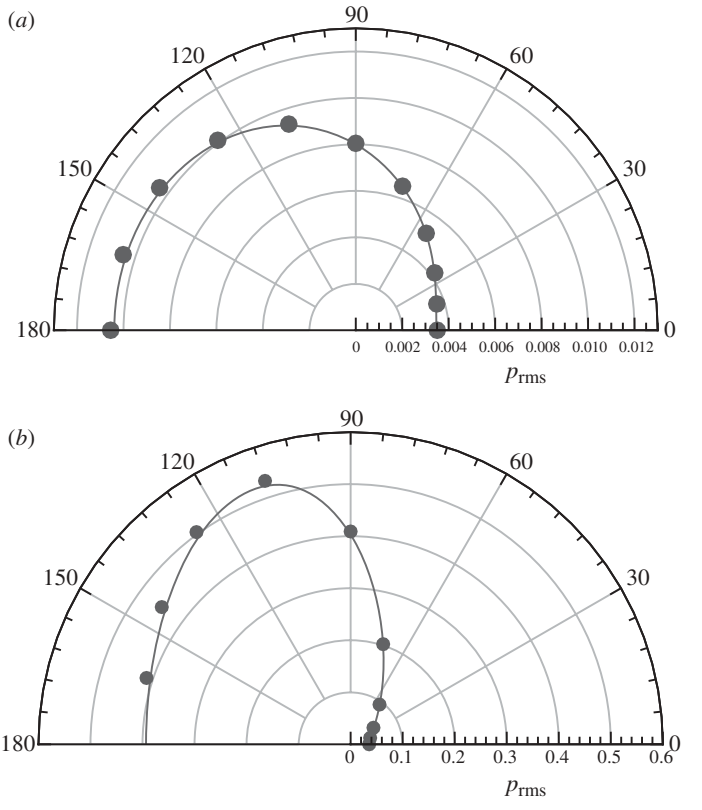

Figure 2. Farfield directivity pattern of a point monopole measured at $r = 340l$, radiating in (a) a flow at $M_0 = 0.5$, and (b) a flow at $M_0 = 0.85$ measured at $r = 340l$. Solid line, exact solution; symbols, FW–H code.

unity. The speed of sound was $340\,\mathrm{m\,s^{-1}}$. Figure 2 shows the directivity pattern of the sound pressure measured in the presence of a uniform mean flow along the the positive x_1-direction for $M_0 = 0.5$ and $M_0 = 0.85$. In this polar plot, the radius indicates the RMS pressure at the observer location, while the polar angle corresponds to the geometrical angle (measured from the x_1 axis) between the source and the observer. In a moving medium, the directivity pattern is directional owing to the convective amplification caused by the mean flow. Convective amplification causes the sound pressure level upstream of the source to be greater than that downstream at the same distance from the source. This convective effect increases with the mean flow Mach number. The ratio of the sound pressure at $\theta = 180^\circ$ (upstream) and that at $\theta = 0^\circ$ (downstream) is equal to the theoretical value of $(1 + M_0)/(1 - M_0)$ with less than 0.3 per cent error.

The FW–H equation applies in principle for observer locations in both the nearfield or the farfield, and involves no farfield approximation. The accuracy of the sound prediction in the nearfield was also verified. Figure 3 shows the directivity pattern measured in the nearfield with microphones located at $r = 5l$. The exact solution and the numerical predictions are in very good agreement. The small deviation from the exact solution is due to the fact that measurements

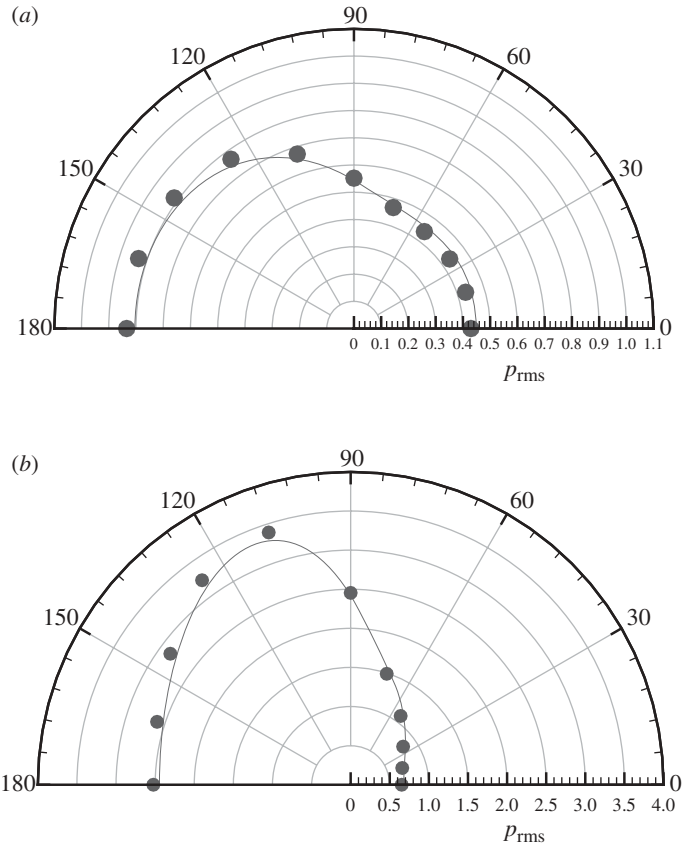

Figure 3. Nearfield directivity pattern of a monopole measured at $r = 5l$, radiating in (*a*) a flow at $M_0 = 0.5$, and (*b*) a flow at $M_0 = 0.85$ (test case 1). Solid line, exact solution; symbols, FW–H code.

were made very close to the FW–H surface, where the size of the panels (mesh cells) is comparable to the distance between the source and the observer. This means that the panels are no longer acoustically compact. A finer surface mesh yielded more accurate results (results not shown here).

(*b*) *Test case 2. Stationary dipole in a moving medium*

The second validation test case is sound radiation from a point dipole in a moving medium. The dipole axis was aligned with the x_2-axis. The velocity potential for such dipole in a mean flow is

$$\phi(\mathbf{x}, t) = \frac{\partial}{\partial x_2}\left\{\frac{A}{4\pi R^*}\exp\left[\mathrm{i}\omega\left(t - \frac{R}{c_0}\right)\right]\right\}. \tag{4.5}$$

The particle velocities and pressure fluctuations were obtained from equations (4.2) and (4.3), respectively. The same potential amplitude, frequency and position as test case 1 were prescribed. Figure 4 shows the directivity pattern

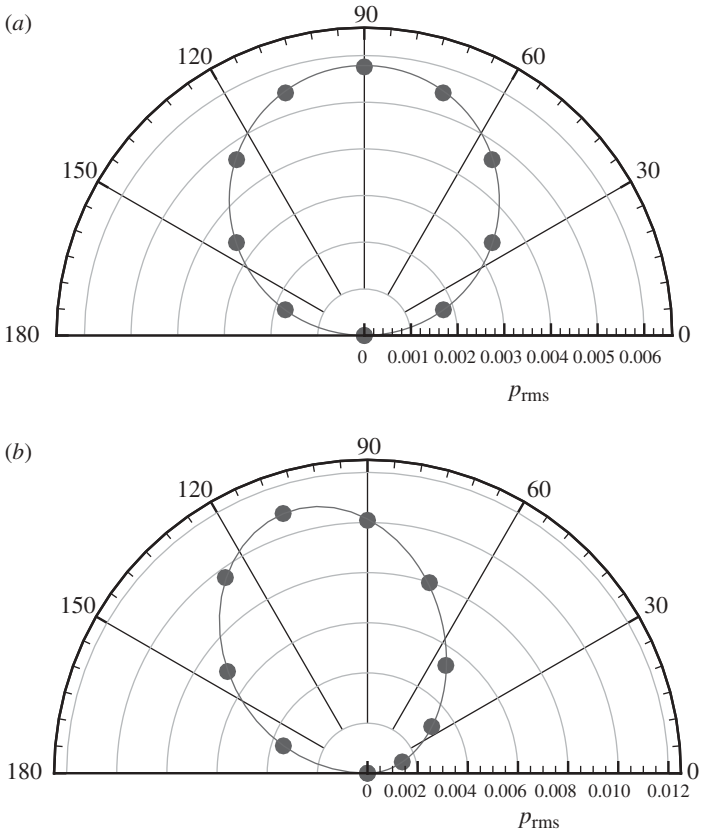

Figure 4. The directivity pattern of a point dipole measured at $r = 30l$, radiating in (a) a medium at rest, and (b) a flow at $M_0 = 0.5$ moving in the positive x_1-direction ($\theta = 0°$). Solid line, exact solution; symbols, FW–H code.

of the sound pressure at $r = 30l$. The mean flow causes the direction corresponding to the maximum acoustic pressure to move in the upstream direction. The FW–H code and the exact solution yield nearly identical results.

(*c*) *Test case 3. Rotating monopole in a moving medium*

The last test case is a rotating monopole radiating in a moving medium as shown schematically in figure 5. This case was designed to validate the accuracy of Formulation 1C to predict the general case of sound radiated by *moving* sources in uniformly moving media. This case features radiation effects similar to those of the thickness source term of a fan or a helicopter rotor blade measured in wind tunnels. A monopole was placed initially at $(0.7l, 0, 0)$, surrounded by an FW–H surface moving with the source. The monopole rotated around the x_3-axis with an angular speed of 2π (rad s^{-1}). The potential amplitude was $A = 1\,\mathrm{m}^2\,\mathrm{s}^{-1}$ and the pulsation frequency was 5 Hz as for the previous test cases. The ambient medium had a Mach number of $M_0 = 0.5$ moving in the positive x_1-direction. Figure 6*a* shows the time history of the sound pressure perceived

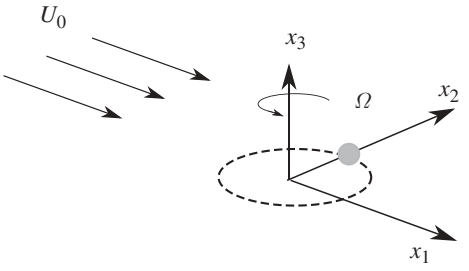

Figure 5. The schematic of a rotating monopole in a moving medium.

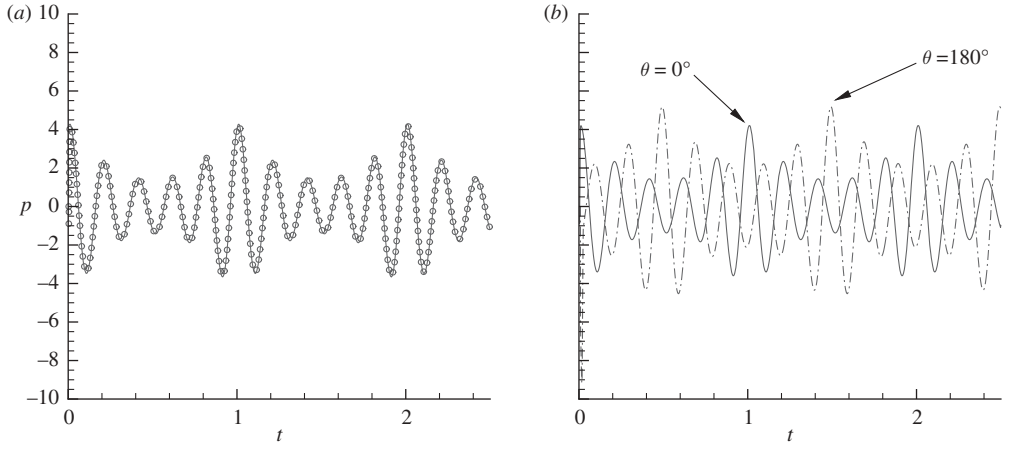

Figure 6. Time history of the sound pressure generated by a rotating monopole in a moving medium (test case). (*a*) At $(2l, 0, 0)$ where the solid line corresponds to the exact solution and symbols represent the results obtained from the FW–H code; (*b*) comparison between the results at $(2l, 0, 0)$, $\theta = 0°$, and at $(-2l, 0, 0)$, $\theta = 180°$.

by an observer located at $(2l, 0, 0)$. Excellent agreement between the exact solution and the farfield prediction confirms the validity of Formulation 1C and its implementation.

The effect of the mean flow is illustrated in figure 6*b*, where the time histories of the sound pressure measured upstream ($\theta = 0°$) and downstream ($\theta = 180°$) of the monopole at a distance of $r = 2\,l$ are compared. As expected, the amplitude of the peak pressure for the upstream observer is greater than that for the downstream observer because of convective amplification. The pressure ratio is no longer $(1 + M_0)/(1 - M_0)$, as in case 2, because of the motion of the monopole.

5. Conclusion

An acoustic analogy formulation based on the convective form of the FW-H equation was introduced. The formulation, called Formulation 1C, was used to simulate wind-tunnel acoustic measurements of stationary or moving sources. The same formulation is also useful for moving-observer problems.

In comparison with the classical non-convective FW–H equation, the temporal derivative of the thickness noise changes to a Lagrangian temporal derivative in the convective FW–H formulation. The monopole (thickness) and dipole (loading) sources also change slightly. The quadrupole term retains the same form as in the classical FW–H equation. The convective FW–H equation was solved using the Green's function suggested by Blokhintsev (1956).

Formulation 1C is amenable to the advanced time approach implementation, which may significantly reduce storage and computation requirements. The validity of formulation 1C and its implementation was demonstrated for the canonical test cases of a monopole and a dipole radiating in a moving medium. A test case for a rotating monopole was also investigated. In all cases, numerical results were in very good agreement with the exact solutions.

This work was sponsored by Exa Corporation. The authors would like to thank Drs David Freed, Frank Perot, Richard Shock from Exa Corporation and Phoi-Tack Lew from McGill University for their help and comments.

Appendix A. Derivation of Formulation 1C in terms of source temporal derivatives

The details of the derivation of the thickness noise in terms of the source temporal derivative, namely equation (3.16), are shown. The derivation of the loading noise term, equation (3.20), follows the same steps, and is not presented.

Consider a general expression of the form

$$I_Q = \frac{\partial}{\partial t}\int_{-\infty}^{t}\int_{\mathbb{R}^3} T(\mathbf{y},\tau)\delta(f)\frac{\delta(g)}{R^*}\mathrm{d}\mathbf{y}\,\mathrm{d}\tau. \tag{A 1}$$

Taking the temporal derivative inside the integral, and using the Leibniz rule, yields

$$I_Q = \int_{-\infty}^{t}\int_{\mathbb{R}^3} T(\mathbf{y},\tau)\delta(f)\frac{\partial}{\partial t}\left(\frac{\delta(g)}{R^*}\right)\mathrm{d}\mathbf{y}\,\mathrm{d}\tau + \int_{\mathbb{R}^3} T(\mathbf{y},t)\delta(f(\mathbf{y},t))\frac{\delta(R/c)}{R^*}\mathrm{d}\mathbf{y}. \tag{A 2}$$

The second integral on the RHS of the above equation is zero. This can be proven as follows. Consider the spherical coordinate system (R^*,ϕ,θ), where

$$\phi = \tan^{-1}\left(\frac{x_3 - y_3}{x_2 - y_2}\right) \tag{A 3}$$

and

$$\theta = \tan^{-1}\left(\frac{\beta\sqrt{(x_2 - y_2)^2 + (x_3 - y_3)^2}}{x_1 - y_1}\right). \tag{A 4}$$

The above transformation can be used to replace y and R in terms of R^*

$$R = \frac{-M_0(x_1 - y_1) + R^*}{\beta^2} = \frac{R^*}{\beta^2}(1 - M_0\cos\theta). \tag{A 5}$$

The second integral can then be recast as

$$I_2 = \lim_{\epsilon \to 0} \int_0^\infty \int_0^\pi \int_0^{2\pi} T(R^*, \phi, \theta, t)\delta(f(R^*, \phi, \theta, t))\delta \times \left(\frac{(R^* - \epsilon)(1 - M_0 \cos\theta)}{\beta^2 c_0} \right) R^* \sin\theta \mathrm{d}R^* \mathrm{d}\theta \, \mathrm{d}\phi. \tag{A 6}$$

The above equation can be further simplified to

$$I_2 = \lim_{\epsilon \to 0} \int_0^\infty \int_0^\pi \int_0^{2\pi} T(R^*, \phi, \theta, t)\delta(f(R^*, \phi, \theta, t)) \times \frac{\beta^2 c}{1 - M_0 \cos\theta} \delta(R^* - \epsilon) R^* \sin\theta \, \mathrm{d}R^* \, \mathrm{d}\theta \, \mathrm{d}\phi. \tag{A 7}$$

Since $R^*\delta(R^* - \epsilon) = \epsilon\delta(\epsilon - R^*)$, the above integral vanishes as $\epsilon \to 0$. Hence

$$I_Q = \int_{-\infty}^{t} \int_{\mathbb{R}^3} T(\mathbf{y}, \tau)\delta(f) \frac{\partial}{\partial t} \left(\frac{\delta(g)}{R^*} \right) \mathrm{d}\mathbf{y} \, \mathrm{d}\tau = \int_{-\infty}^{t} \int_{\mathbb{R}^3} \frac{\partial}{\partial t} \left[T(\mathbf{y}, \tau)\delta(f) \frac{\delta(g)}{R^*} \right] \mathrm{d}\boldsymbol{y} \, \mathrm{d}\tau. \tag{A 8}$$

The above identity means that we can take the temporal derivative inside the integral. The integrals of equation (3.10) are then contracted to obtain equation (3.14), and the differential operator is moved inside the integral to obtain

$$4\pi p'_T = \int_{f=0} \frac{\partial}{\partial t} \left[\frac{Q_j n_j}{R^*(1 - M_R)} \right]_{\tau_\mathrm{e}} \mathrm{d}\boldsymbol{\eta} - M_0 \int_{f=0} \frac{\partial}{\partial t} \left[\frac{\tilde{R}_1 Q_j n_j}{R^*(1 - M_R)} \right]_{\tau_\mathrm{e}} \mathrm{d}\boldsymbol{\eta} - U_0 \int_{f=0} \left[\frac{\tilde{R}_1^* Q_j n_j}{R^{*2}(1 - M_R)} \right]_{\tau_\mathrm{e}} \mathrm{d}\boldsymbol{\eta}. \tag{A 9}$$

The last step is to transform the differentiation with respect to observer time into a differentiation with respect to source time,

$$\left(\frac{\partial}{\partial t} \right)_x = \left[\frac{\partial \tau}{\partial t} \frac{\partial}{\partial \tau} \right]_{\tau_\mathrm{e}}, \tag{A 10}$$

where subscript x means that x is kept constant in the above differentiation. Since emission time τ_e is the root of $g(\mathbf{x}, t; \mathbf{y}, \tau) = 0$,

$$\frac{\partial}{\partial t} \left([g(\mathbf{x}, t; \mathbf{y}, \tau)]_{\tau_\mathrm{e}} \right)_x = 0 = \frac{\partial \tau}{\partial t} - 1 + \frac{\partial y_i}{\partial t} \frac{\partial R}{\partial y_i}, \tag{A 11}$$

which yields

$$\frac{\partial}{\partial t} = \left[\frac{1}{1 - M_R} \frac{\partial}{\partial \tau} \right]_{\mathrm{ret}}. \tag{A 12}$$

Using the above identity, the final form of the thickness noise can be deduced as presented in equation (3.16). Similarly, the loading noise takes the form that is presented in equation (3.20).

References

Blokhintsev, D. 1956 Acoustics of a nonhomogeneous moving medium. NACA TM-1399. See http://ntrs.nasa.gov.

Brentner, K. S. 1986 Prediction of helicopter discrete frequency noise-a computer program incorporating realistic blade motions and advanced acoustic formulation. NASA TM-87721. See http://ntrs.nasa.gov.

Brentner, K. S. 1997*a* Numerical algorithms for acoustic integrals with examples for rotor noise prediction. *AIAA J.* **35**, 625–630. (doi:10.2514/2.182)

Brentner, K. S. 1997*b* An efficient and robust method for predicting helicopter high-speed impulsive noise. *J. Sound Vib.* **203**, 87–100. (doi:10.1006/jsvi.1996.0834)

Brentner, K. S. & Farassat, F. 1998 An analytical comparison of the acoustic analogy and Kirchhoff formulation for moving surfaces. *AIAA J.* **36**, 1379–1386. (doi:10.2514/2.558)

Brentner, K. S. & Farassat, F. 2003 Modeling aerodynamically generated sound of helicopter rotors. *Prog. Aero. Sci.* **39**, 83–120. (doi:10.1016/S0376-0421(02)00068-4)

Brès, G. A., Brentner, K. S., Perez, G. & Jones, H. E. 2004 Maneuvering rotorcraft noise prediction. *J. Sound Vib.* **275**, 719–738. (doi:10.1016/j.jsv.2003.07.005)

Casalino, D. 2003 An advanced time approach for acoustic analogy predictions. *J. Sound Vib.* **264**, 583–612. (doi:10.1016/S0022-460X(02)00986-0)

Curle, N. 1955 The influence of solid boundaries upon aerodynamic sound. *Proc. R. Soc. Lond. A* **231**, 505–514. (doi:10.1098/rspa.1955.0191)

Di Francescantonio, P. 1997 A new boundary integral formulation for the prediction of sound radiation. *J. Sound Vib.* **202**, 491–509. (doi:10.1006/jsvi.1996.0843)

Farassat, F. 1975 Theory of noise generation from moving bodies with an application to helicopter rotors. NASA Tech. Rep. R-451. Hampton, VA: Langley Research Center.

Farassat, F. 1994 Introduction to generalized functions with applications in aerodynamics and aeroacoustics. NASA-TP-3428, corrected April 1996. See http://ntrs.nasa.gov.

Farassat, F. 2000 Introduction to generalized functions with applications in aerodynamics and aeroacoustics. *J. Sound Vib.* **230**, 460–462. (doi:10.1006/jsvi.1999.2580)

Farassat, F. & Myers, M. K. 1988 Extension of Kirchoff's formula to radiation from moving surfaces. *J. Sound Vib.* **123**, 451-460. (doi:10.1016/S0022-460X(88)80162-7)

Farassat, F. & Succi, G. P. 1980 A review of propeller discrete frequency noise prediction technology with emphasis on two current methods for time domain calculations. *J. Sound Vib.* **31**, 399–419. (doi:10.1016/0022-460X(80)90422-8)

Ffowcs Williams, J. E. & Hawkings, D. 1969 Sound generation by turbulence and surfaces in arbitrary motion. *Phil. Trans. R. Soc. Lond. A* **264**, 321–342. (doi:10.1098/rsta.1969.0031)

Howe, M. S. 1998 *Acoustics of fluid-structure interactions*. Cambridge, UK: Cambridge University Press.

Leishman, J. G. 1996 Aeroacoustics of 2-D and 3-D blade vortex interaction using the indicial method. *Proc. 52nd Annual Forum American Helicopter Society*, Washington, DC: American Helicopter Society.

Lighthill, M. J. 1952 On sound generated aerodynamically. I. General theory. *Proc. R. Soc. Lond. A* **211**, 564–587. (doi:10.1098/rspa.1952.0060)

Lighthill, M. J. 1954 On sound generated aerodynamically. II. Turbulence as a source of sound. *Proc. R. Soc. Lond. A* **222**, 1–32. (doi:10.1098/rspa.1954.0049)

Lockard, D. 2002 A comparison of Ffowcs Williams-Hawkings solvers for airframe noise applications. In *Proc. of the 8th AIAA/CEAS Aeroacoustics Conference and Exhibition*, pp. 2002–2580. Washington, DC: AIAA.

Lyrintzis, A. S. 1994 Review: the use of Kirchhoff's method in computational aeroacoustics. *J. Fluids Eng.* **116**, 665–676. (doi:10.1115/1.2911834)

Lyrintzis, A. S. 2003 Surface integral methods in computational aeroacoustics. From the (CFD) near-field to the (Acoustic) far-field. *Int. J. Aeroacoust.* **2**, 95–128. (doi:10.1260/147547203322775498)

Lyrintzis, A. S. & Xue, Y. 1997 Towards a versatile Kirchhoff's method code. *AIAA J.* **35**, 198–200. (doi:10.2514/2.7434)

Morgans, A. S., Karabasov, S. A., Dowling, A. P. & Hynes, T. P. 2005 Transonic helicopter noise. *AIAA J.* **43**, 1513–1524. (doi:10.2514/1.6679)

Morino, L. 1974 A general theory of unsteady compressible potential aerodynamics. NASA CR-2464. See http://ntrs.nasa.gov.

Morino, L. 1985 Mathematical foundations of integral methods. In *Computational methods in potential aerodynamics* (ed. L. Morino), pp. 271–291. New York, NY: Springer.

Renardy, M. & Rogers, R. C. 2004 *An introduction to partial differential equations*. New York, NY: Springer.

Wells, V. L. & Han, A. Y. 1995 Acoustics of a moving source in a moving medium with application to propeller noise. *J. Sound Vib.* **184**, 651–663. (doi:10.1006/jsvi.1995.0339)